Characterization of the Electroencephalogram of Microsleep Using Self-Organized Feature Maps

David Sommer[1], Martin Golz[1], Udo Trutschel[2], Chris Ramsthaler[1, 2], Martin Moore-Ede[2]
[1]University of Applied Sciences, Department of Computer Science, Postfach 182
Schmalkalden, D-98574, Germany
{sommer, golz}@informatik.fh-schmalkalden.de
[2]Circadian Technologies Inc., 24 Hartwell Avenue
Lexington, MA 02421, USA

Abstract

Slow eye movements were detected in the electro-oculogram of eleven subjects during nighttime driving simulations. Simultaneously recorded EEG segments were transformed to the frequency domain with discrete Fourier transform. A subsequent clustering without the common summation in spectral bands sought to analyze how many types of EEG segments were distinguishable. Self-organizing maps were applied for clustering. The visualization of the winner histogram showed no evidence. Therefore the analysis of the U-matrix together with the watershed transformation, a method from image processing, resulted in separable clusters. As in many other procedures, the number of clusters was determined with one threshold parameter. Best results were obtained with 9 clusters; two of them had spectral densities mainly in the alpha1 band. Other clusters were found in the alpha2, theta and delta bands.

Keywords: Slow eye movements, EEG, clustering, self-organizing feature map, U-matrix, watershed transformation

1 Introduction

As the alertness of a subject deteriorates during extended periods of night work, the probability of short attention lapses increases [1]. Sleepiness on night shift is likely to play an important role in the occurrence of nighttime accidents [2-5]. Torsvall et al. [6] report in their study that one of five industrial shift workers fell asleep during work, mainly in the early morning. There have been several attempts to study sleepiness on night shift in laboratory studies [7-9] and also in field studies [6,10-12] using polysomnographic recordings.

Akerstedt et al. [11] show that with increasing working time subject rated sleepiness strongly increases and EEG shows a significant but moderate increase of hourly mean spectral power density in the alpha band (7.5 ... 12.5 Hz). Though hourly averaged power in the theta band (3.5 … 7.5 Hz) is not affected, they report that very short burst-like theta activity could be observed during a short nap. Short alpha activity before, during and after a short nap could also be observed. The attention-loss phase, sometimes called microsleep [24], is characterized by a transition from the struggle to remain awake to an involuntary short sleep episode. This phase is also associated with an increased activity of slow eye movements (SEM) [13,14]. SEMs are slow (f = 0.2 ... 0.7 Hz) excursions ($u > 100\ \mu V$) of the EOG, lasting for more than 1 sec [9], remaining sometimes during sleep stage 1.

Our investigations were focused on the spectral characterization of EEG during SEM without using the common spectral bands in a nonlinear clustering procedure. We used Kohonen's self-organized feature maps combined with an improved method to estimate the number of spectral EEG clusters.

2 Experiments

Eleven subjects (3 females, 8 males) aged between 19 and 36 years participated in an overnight driving simulator study. Their task was intentionally monotonous, simply to avoid major lane deviations. One driving session of 25 min length was carried out, every hour from 1 a.m. until 7 a.m. The face of the driver and the region of the right eye were video-

recorded separately. EEG was recorded in two unipolar and two bipolar recordings (C3-A2, C4-A1, O1-C3, O2-C4), as were EOG (oblique) and ECG.

3 Analysis

EEG and EOG analog signals were recorded with an Oxford Medilog system, filtered with a 30 Hz lowpass filter, and digitized at a rate of 64 samples per second [15,16]. SEMs were automatically recognized using the cross correlation function between the EOG signal and a sine-signal having a duration of 8 sec. If the value of the correlation function exceeded an empirical selected threshold of 0.75 for three periodically spaced values in a row, we assumed that SEM was detected. The frequency and the amplitude of the sine-signal were estimated by fitting the sine-signal to 15 SEM signals from three subjects obtained through visual scoring. Figure 1 shows the cross correlation function computed with 0.5 sec time steps as a white line.

Each detected SEM was confirmed by visual scoring of the recorded digital video. The video showed that most SEMs occur with closed or half closed-eyes. Occasionally we observed SEM with eyes open accompanied by blank staring. The bipolar EEG recorded at O2-C4 was segmented to a length of 2 sec for a recognized SEM event.

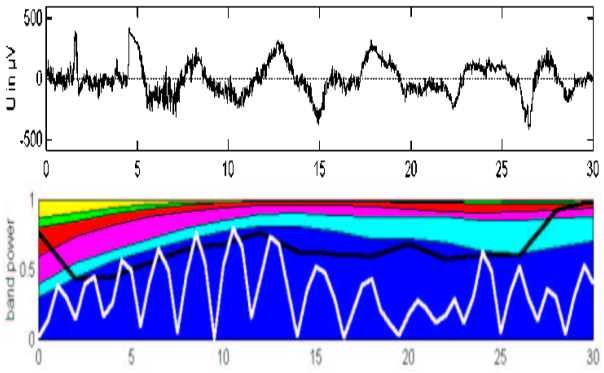

Figure 1: EOG of a typical SEM event in the early morning upper chart: EOG; lower chart: relative spectral power density of the EOG in the following bands (from bottom to top, all values in Hz) 0.1-0.4, 0.4-0.6, 0.6-0.8, 0.8-1.2, 1.2-1.5, 1.5-5.0; white line: cross correlation function; black line: total power density

Before applying the fast Fourier transform, any linear trends in the EEG segments were eliminated and a Welch window was applied to reduce bias effects due to nonstationarity and sidelobe effects [17]. The reduction of the total power density due to the windowing was corrected using the Parceval theorem. The error of each spectral component of stochastic signals could reach 100%. Therefore the Welch method of averaging the periodogram over shifted windows was used. We were able to reduce the variance of the Welch periodogram by a factor of n^{-1}, where n is the number of shifted windows. In [17] the optimal overlap was estimated at 65% for a Gaussian process.

Figure 1 shows a sine-shaped EOG (upper chart) indicating SEM occurring in the early morning (6:14 a.m.) during a prolonged eye closure of 15 seconds. This event is also characterized by a sharp increase of EOG relative spectral power density in the lowest range (0.1 ... 0.4 Hz) (lower chart). Total spectral power density (black line, lower chart) is not strongly affected.

Figure 2 shows the associated EEG. Absolute spectral power density (black line, lower chart) and relative power in the alpha2-band (fourth stacked band from the bottom, lower chart) increase during SEM. The spectral components for EEG below 2 Hz and above 25 Hz were disregarded for cluster analysis to restrict the number of variables. These spectral components have the worst signal-to-noise ratio.

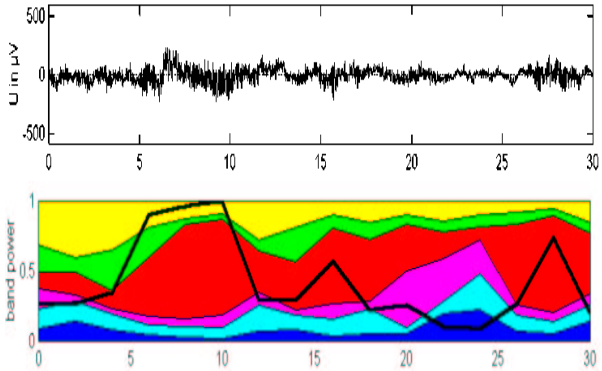

Figure 2: EEG of a typical SEM event in the early morning upper chart: EEG; lower chart: relative spectral power density in the delta, theta, alpha1, alpha2, beta1, beta2 bands (from bottom to top); black line: total power density

The input vectors for the following analysis consisted of 47 spectral components (2 to 25 Hz; 0.5 Hz steps). A principal component analysis (PCA) was routinely computed. There was no reason to assume input vectors in a linear subspace, because the last ten principal components have a residual variance of about 8%. A Scree test indicated 13 principal components, but they explained only 30% of the total variance.

4 Clustering of the EEG-Segments

We used all 47 variables for the self-organizing feature maps (SOM) [18] to perform a cluster analysis. SOM is a prototype vector-based neural network. Using the principle of competitive learning, the prototype vectors can be adapted to the probability density function of the input vectors. This paradigm is also known as vector quantization. The similarity between the input vector $\mathbf{x}$ and the prototype vector $\mathbf{w}$ was calculated using Euclidian distance. During training an arbitrary prototype vector $\mathbf{w}_j$ is updated at iteration index t by:

$$\Delta \mathbf{w}_j(t) = \eta(t)\, h_{cj}(t)\, [\mathbf{x}(t) - \mathbf{w}_j(t)] \qquad (1)$$

Where $\eta(t)$ is a learning rate factor decreasing during training and $h_{cj}(t)$ is a neighborhood function between $\mathbf{w}_c$, the prototype vector winning the competition, and the prototype vector $\mathbf{w}_j$. The neighborhood function $h_{cj}(t)$ also decreases during training. The neighborhood relationships are defined by a topological structure and are fixed during training. We used a two-dimensional tetragonal relationship. In the final phase of training, the fine-adjustment phase [19], the neighborhood radius is very small, leading to updates of the winning prototype vectors $\mathbf{w}_c$ and of their nearest neighbors.
In the case of a one-dimensional topological structure it can be shown [19] that the training rule (Eq.1) leads to an approximation of a monotonous function of the probability density function of the input vectors. The two-dimensional topology results in a compromise between a density approximation and a minimal mean squared error of vector quantization [19].

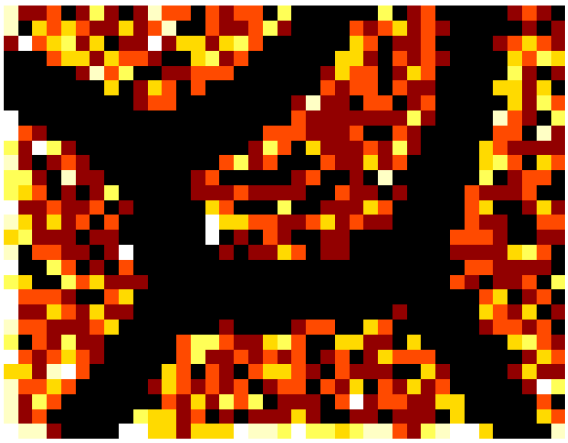

Figure 3a: Relative winner frequency for a SOM with 30x40 neurons for Gaussian mixture data

For existing compact regions of input vectors and existing density centers, as for Gaussian mixtures, the evaluation of the relative winner frequency of the prototypes leads to a visualization of clusters. Figure 3a shows such a gray-level-coded winner histogram. Five areas with increased winner frequency are evident.

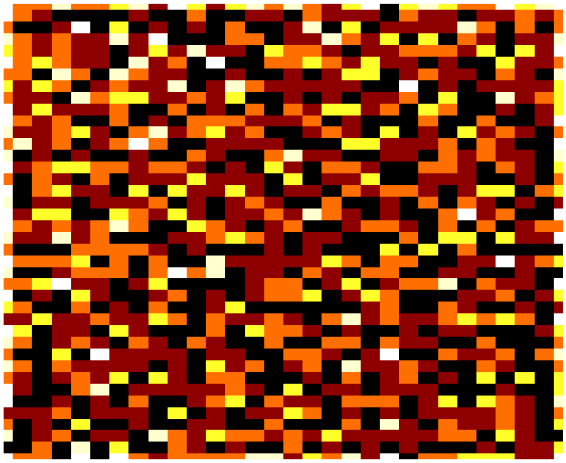

Figure 3b: Relative winner frequency for a SOM with 30x40 neurons for SEM-EEG data

The Gaussian mixture data were generated by defining five cluster centers and five covariance matrices and adding normal distributed noise in a 47-dimensional space, as in our experimental data set. The estimated total covariance matrix of the generated data set and of the experimental data set was nearly the same.

The black colored units in Figure 3a are never-winning neurons (dead neurons), which make it easy to distinguish clusters. Figure 3b shows the relative winner frequency for the experimental data set. Distinguishing regions with increased winner frequency is not possible.

But the SOM has a lot of additional information. For example, the distance between topological neighboring prototype vectors in the feature space can be computed. In the case of topology preservation, these prototype vectors remain neighbors also in the output space (the two-dimensional map) [20]. If the distance between two neighboring prototypes is small, then they probably represent one cluster. Otherwise they probably represent different clusters. The visualization of the distances between neighboring prototype vectors was introduced as the unified distance matrix (U-matrix) [21]. In a two-dimensional tetragonal topology, the U-matrix is calculated in n_X columns and n_Y rows.

For every prototype vector $\mathbf{w}_{x,y}$, where x and y are the indices of the topological structure, the Euclidian distances dx and dy between two neighbors and the distance dxy to the next but one neighbor is calculated:

$$dx(x,y) = \left\| \mathbf{w}_{x,y} - \mathbf{w}_{x+1,y} \right\| \quad (2)$$

$$dy(x,y) = \left\| \mathbf{w}_{x,y} - \mathbf{w}_{x,y+1} \right\| \quad (3)$$

$$dxy(x,y) = \frac{1}{2}\left(\frac{\left\| \mathbf{w}_{x,y} - \mathbf{w}_{x+1,y+1} \right\|}{\sqrt{2}} + \frac{\left\| \mathbf{w}_{x,y+1} - \mathbf{w}_{x+1,y} \right\|}{\sqrt{2}} \right) \quad (4)$$

$$U = \begin{bmatrix} du(1,1) & dx(1,1) & du(2,1) & \dots & du(n_x,1) \\ dy(1,1) & dxy(1,1) & dy(2,1) & \dots & dy(n_x,1) \\ du(1,2) & dx(1,2) & du(2,2) & \dots & du(n_x,2) \\ dy(1,2) & dxy(1,2) & dy(2,2) & \dots & dy(n_x,2) \\ \vdots & \vdots & \vdots & \ddots & \vdots \\ du(1,n_y) & dx(1,n_y) & du(2,n_y) & \dots & du(n_x,n_y) \end{bmatrix} \quad (5)$$

The distance du was calculated using the mean over eight surrounding distances. With four distances for each neuron dx, dy, dxy and du (Figure 4), the $(2n_X - 1) \times (2n_Y - 1)$ U-matrix is well defined.

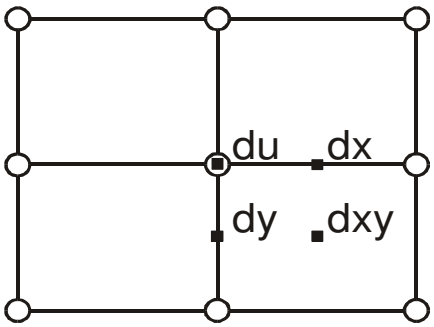

Figure 4: Definition of the U-matrix and localization on the tetragonal topological structure, shown for the neuron in the center only. Circles: positions of neurons; black squares: positions of U-matrix elements

The U-matrix elements were mapped on a gray scale. Light gray levels indicate low values, and dark gray-levels indicate high values.

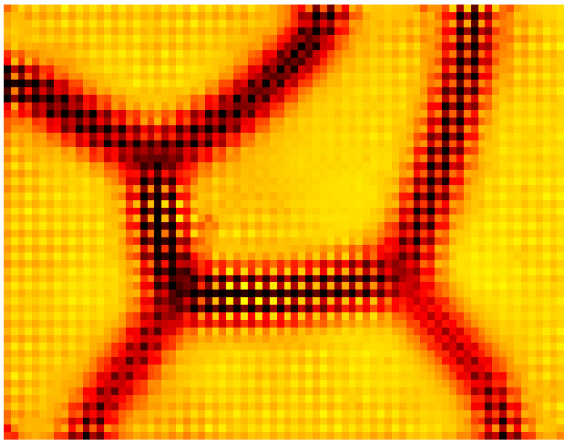

Figure 5a: U-matrix for SOM from Figure 3a

Scoring the U-matrix of Gaussian mixture data (Figure 5a) leads visually to five clusters. As expected, the cluster regions on the map are regions of small distances between the prototype vectors, which are separated by small regions of large distances. The U-matrix of the SEM-EEG data (Figure 5b) has much more complexity, and it is difficult to determine borders.

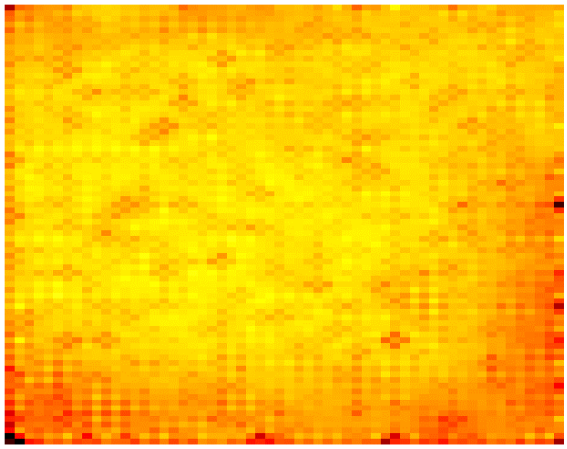

Figure 5b: U-matrix for SOM from Figure 3b

Costa et al. [22] propose an automatic segmentation of the U-matrix using the watershed algorithm of gray scale image processing [23]. Regarding high values as mountains and low values as valleys, the algorithm can be illustrated by flooding the valleys with water; watersheds will be built up where the water converges (Figure 6). This algorithm leads to closed borders. It's not difficult to evaluate the number of clusters. All prototype vectors in one segmented region represent

one cluster, and the fusion of their Voronoi sets leads to all items of a cluster.

It's difficult to choose suitable initial values for each reservoir; otherwise a generation of many segments is unavoidable [22]. The number of segments can be reduced during initialization by the threshold parameter h_{min}. All values which are lower than h_{min} are assigned to the same value as h_{min}.

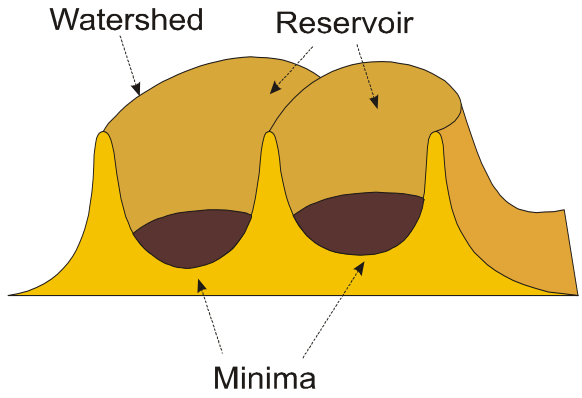

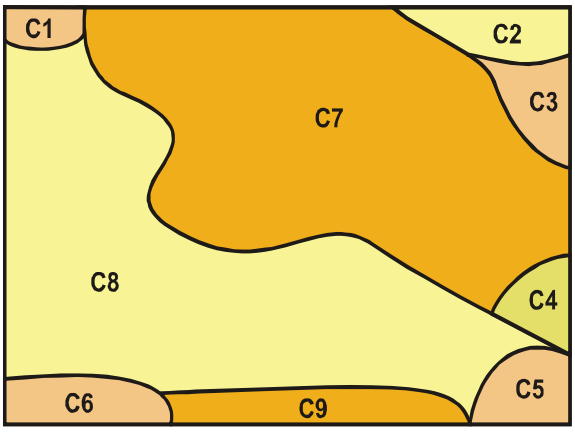

Figure 7: U-matrix from Figure 5b after watershed Transformation

5 Number of Clusters

The results of segmentation are dependent on the size of the SOM. With a relatively large number of prototype vectors many clusters are obtained. Smoothing the gray level function with a two-dimensional filter reduces the risk of multiple segmentations.

In several regions of the U-matrix (Figure 5a, 5b) black-and-white textures are observable. They describe relatively large differences between dx and dy and are connected with local stretchings of the SOM along one topological coordinate.

If the dx elements of the U-matrix, for example, are visualized only, some segment borders disappear. Up to now the following defaults were used:

- use of function du(x,y)
- 3x3-Gaussian filtering
- watershed transformation

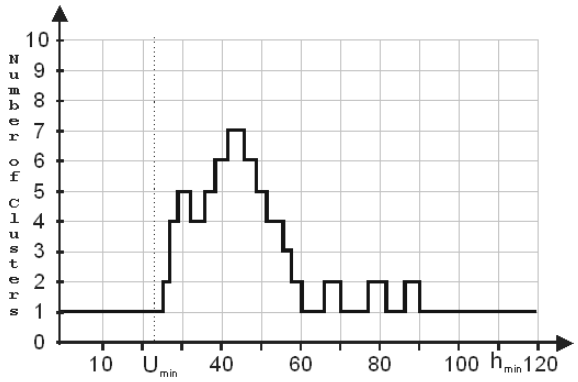

Figure 8a: Number of clusters vs. h_{min} for the U-matrix of Figure 5b with generation of new regions [22].

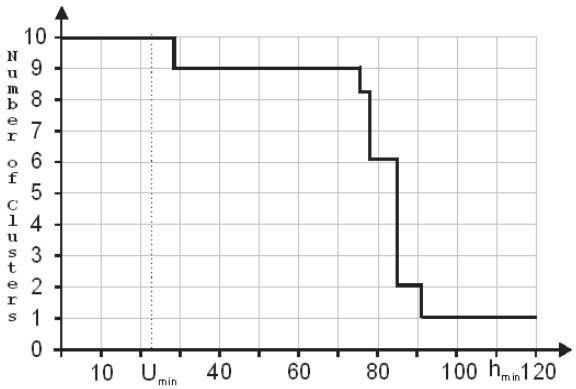

Figure 8b: Number of clusters vs. h_{min} for the U-matrix of Figure 5b without generation of new regions.

The segmentation was repeated many times with increasing threshold parameter h_{min} [22] (Figure 8a). No plateau in the number of clusters was detectable. Therefore we propose a modification allowing the generation of new minima regions during flooding. For the most extended plateau we obtained 9 clusters (Figure 8b).

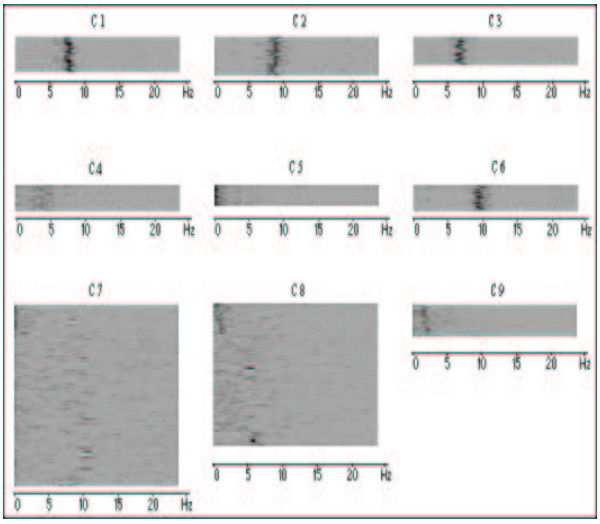

Figure 9: All 1652 input vectors grouped in 9 different clusters; horizontal: frequency; vertical: item; gray scale: spectral power density.

6 Results

The 9-cluster solution of the described clustering and segmentation procedure is shown in Figure 7. The segments contain different number of prototype vectors. The fusion of their Voronoi sets, mentioned above, leads to the clusters (Figure 9). Cluster 1 and 2 contain input vectors with large magnitudes in the alpha1 band (7.5-10.5 Hz), cluster 6 in the alpha2 band (10.5-12.5 Hz), cluster 3 in the theta band (3.5-7.5 Hz) and cluster 9 in the delta band (1.0-3.5 Hz). In contrast to the usual summation in frequency bands, more details are available. The input vectors of cluster 1 and 2, for example, are large in the same spectral band, but they differ in the magnitude range and differ in other spectral bands.

From Figure 9 one may get the visual impression of homogeneous clusters, with the exception of cluster 7 and 8.

An advantage of the described method is the relatively low number of free parameters and the ability to reproduce the results. A comprehensive validation of the results remains to be carried out.

Acknowledgments

We want to thank T. J. Minnes for his excellent translation support.

References

[1] Akerstedt, T; Gillberg, M; Subjective and objective sleepiness in the active individual; *Int J Neuroscience*, 36, 9, 1993, 1007-1017.

[2] Lauber, JK; Kayten, PJ; Sleepiness, circadian dysrhythmia, and fatique in transportation system accidents; *Sleep*, 11, 1988, 503-512.

[3] Mitler, MM; Caskardon, MA; Czeisler, CA; Dement, WC; Dinges, DF; Graeber, RC; Catastrophes, sleep and public policy. Census report; *Sleep*, 11, 1988, 100-109.

[4] Prokop, O; Prokop, A; Ermüdung und Einschlafen am Steuer; *Verkehrsmedizin*, 1, 1955, 19-30 (in German).

[5] Moore-Ede, M; *The twenty-four hour society - understanding human limits in a world that never stops*; Addison-Wesley, Reading, MA; 1993.

[6] Torsvall, L; Akerstedt, T; Gillander, K; Knutsson, A; Sleep on the night shift. 24-hour EEG monitoring of spontaneous sleep/awake behavior; *Psychophysiology*, 26 (3), 1989, 352-358.

[7] O'Hanlon, JF; Kelly, GR; Concurrence of electroencephalographic and performance changes during a simulated radar watch and some implications for the arousal theory of vigilance; in Mackie, RR (ed); Vigilance: theory, operational performance and physiological correlates; Plenum Press, New York, 1976, 189-202.

[8] Heitmann, A; Stampi, C; Machi, M; Methodological aspects of continuous EEG recording for the assessment of driver alertness; *Proc 11th Int Symp Night & Shiftwork*, Melbourne, 1994, 41-42.

[9] Heitmann, A; Stampi, C; Machi, M; Techniques for assessment of driver alertness from the EEG alpha frequency band; *J Sleep Res*, 3, Suppl.1, 1994, 103.

[10] Torsvall, L; Akerstedt, T; Sleepiness on the job: Continuously measured EEG changes in train drivers; *Electroenceph Clin Neurophysiol*, 66, 1987, 502-511.

[11] Akerstedt, T; Kecklund, G; Knutsson, A; Manifest sleepiness and the spectral content of the EEG during shift work; *Sleep*, 14 (3), 1991, 221-225.

[12] O'Hanlon, JF; Kelly, GR; Comparison of performance and physiological changes between drivers who perform well and poorly during prolonged vehicular operation; in Mackie, RR (ed); Vigilance: theory, operational performance and physiological correlates; Plenum Press, New York, 1976, 87-111.

[13] Kuhlo, W; Lehmann, D; Das Einschlaferleben und seine neurophysiologischen Korrelate; *Arch Psychiat Z ges Neurol*, 205, 1964, 687-716 (in German).

[14] Liberson, WT; Liberson, CT; EEG recordings, reaction times, eye movements, respiration and mental content during drowsiness; *Proc Soc Biol Psychiat*, 19, 1966, 295-302.

[15] Medilog 9000-II; Technical Reference; Oxford Medical Systems Ltd., 1984.

[16] Declerck, AC; Martens, WLJ; Schlitz, AM; Evaluation of ambulatory EEG cassette recording; in Stefan, H Burr, W (eds); *EEG Monitoring*; Gustav Fischer, Stuttgart, 1982, 29-35.

[17] Marple Jr, SL; Digital spectral analysis with applications; *Prentice Hall, Englewood Cliffs*, 1987.

[18] Kohonen, T; Self-organized formation of topologically correct feature maps; *Biol Cybern*, 43, 1982, 59-69.

[19] Kohonen, T; *Self-organizing maps, 3rd ed.*; Springer, Berlin, 2000.

[20] Villmann, T; *Topologieerhaltung in selbstorganisierenden neuronalen Merkmalskarten*; PhD thesis, University of Leipzig, 1996 (in German).

[21] Ultsch, A; Siemon, HP; Exploratory data analysis: Using Kohonen networks on transputers; Univ. of Dortmund, *Technical Report 329*, Dortmund, Dec. 1989.

[22] Costa, Netto; Automatic data classification by a hierarchy of self-organizing maps; *InProc. of the IEEE*, 1999.

[23] Vincent, L; Soille, P; Watersheds in digital spaces: An efficient algorithm based on immersion simulation; *IEEE Transaction on Pattern Analysis and Machine Intelligence*, 1991.

[24] Thorpy, MJ; Yager, J; *The encyclopedia of sleep and sleep disorders*; NewYork: Facts on File, 1991.